Journal of Engineering Mathematics (2005) 51: 261–282
DOI 10.1007/s10665-004-3692-y
© Springer 2005

Local integro-differential equations with domain elements for the numerical solution of partial differential equations with variable coefficients

V. SLADEK, J. SLADEK and Ch. ZHANG[1]
Institute of Construction and Architecture, Slovak Academy of Sciences, 845 03 Bratislava, Slovak Republic (Vladimir.Sladek@savba.sk); [1]Department of Civil Engineering, University of Applied Sciences Zittau/Görlitz, D-02763 Zittau, Germany (c.zhang@hs-zigr.de)

Received 24 October 2003; accepted in revised form 19 July 2004

Abstract. A new approach (Domain-Element Local Integro-Differential-Equation Method – DELIDEM) is developed and implemented for the solution of 2-D potential problems in materials with arbitrary continuous variation of the material parameters. The domain is discretized into conforming elements for the polynomial approximation and the local integro-differential equations (LIDE) are considered on subdomains determined by domain elements and collocated at interior nodes. At the boundary nodes, either the prescribed boundary conditions or the LIDE are collocated. The applicability and reliability of the method is tested for several numerical examples.

Key words: continuous non-homogeneity, finite element, local integro-differential equations, PDEs with variable coefficients, potential problems

1. Introduction

In many engineering materials, especially functionally graded materials (FGMs), the physical properties are characterized in continuum theories by position-dependent material coefficients or in other words, many engineering materials are practically non-homogeneous. Hence, the development of efficient numerical methods is required and subsequently computer codes incorporating the variation of material coefficients. In the past decade, much attention has been paid to FGMs because of their excellent thermal and mechanical properties. Owing to the continuous change in the material composition and gradation, the material performance can be tailored and optimized to fulfill particular service requirements. Subjects related to the processing, characterization and potential applications of FGMs can be found in the review articles by Hirai [1] and Paulino *et al.* [2] as well as in the monographs by Suresh and Martensen [3] and Miyamoto *et al.* [4].

Mathematically speaking, boundary-value problems (BVPs) for FGMs are described by partial differential equations (PDEs) with variable coefficients. It is beyond the scope of this paper to give a comprehensive review on the literature devoted to the analytical and numerical methods for the solution of such PDEs. Both the well-established finite-element method (FEM) and the boundary-element method (BEM) or boundary-integral-equation method (BIEM) have to be modified and extended from homogeneous materials to FGMs. Special graded elements have been proposed by Kim and Paulino [5] to improve the conventional FEM for FGMs. It is well known that the FEM as a domain-type discretization method has some advantages over the BEM for problems with material non-homogeneity or

nonlinearities. Strictly speaking, the pure boundary-element formulation, resulting in only the boundary being discretized, is applicable to BVP only when the fundamental solutions or the Green's functions of the governing PDEs are available. Nevertheless, the boundary-integral-equation formulation has been applied also to BVP in non-homogeneous materials by using the boundary elements and the domain cells simultaneously in the so-called boundary-domain formulations (see, *e.g.*, [6,7]). However, the simultaneous use of both the boundary elements and the domain cells is inherently inconsistent because the boundary densities are assumed to be mutually independent over the boundary element, while the gradients of the primary field are not independent of its approximation within the domain cell [8]. Despite this fact, boundary-domain formulations have been employed in BIEM, especially for non-homogeneous and nonlinear problems, but with certain loss of efficiency as compared with the pure boundary-integral formulation.

The attraction of the dimensional reduction in pure boundary-element formulations motivated much research work on the derivation of fundamental solutions for PDEs with variable coefficients. Some success has been achieved on this subject (see, *e.g.*, [9–17]), but often with strong restrictions on the functional dependence of the variable coefficients representing the material non-homogeneity. Moreover, the derived fundamental solutions can be expressed only in terms of transcendental functions and/or integrals which are too complex to be suitable for numerical implementation and hence make the BIEM more cumbersome.

Owing to the dimensional reduction, pure BEM formulations are advantageous over the standard FEM, especially for stress-concentration problems such as notch or crack problems, and problems with free moving boundaries when a remeshing is required. Avoiding remeshing is one of the most important motivations for the great effort towards developing meshfree or meshless implementations of both the integral equations and variational approaches employed in FEM. Among many meshless methods proposed in the literature, the meshless local integral-equation method (LIEM) involving the moving least-squares (MLS) approximation seems to be very promising in dealing with BVP in non-homogeneous materials with a continuous variation of material parameters [8,18–23]. A disadvantage of this approach is that it involves three free parameters (namely the radius of sub-domains, the radius of the influence domain and a parameter used in the weight functions for the MLS approximation) which should be properly selected.

Recently, further attention has been devoted to extending the applicability of integral-equations-based formulations for the solution of BVPs when the fundamental solution is not available in a simple way with the purpose of getting a formulation resulting in a sparse system matrix like in FEM. One such proposal concerns a combination of the global and local integral equations implemented either by the standard finite-size discretization elements or the MLS approximation [8,24–27]. Mikhailov [28] and Mikhailov and Nakhova [29] proposed to use localized boundary-domain-integral equations for solution BVPs governed by PDEs with variable coefficients. In their formulations the fundamental solution is replaced by a parametrix (Levi function).

In this paper, we aim to demonstrate that the numerical implementation of the approach based on the local integro-differential equations (LIDE) and domain-element approximation of the field variable [8] yields satisfactory results when solving 2-D potential problems in media with continuously varying material coefficients. The use of domain elements for discretization may appear to be a pre-processing disadvantage in problems requiring remeshing. This, then, is the price to be paid for getting a sufficiently simple, general and reliable (accurate and numerically stable) computational method. The simplicity is borne out by the use of a simple fundamental solution (expressed by elementary functions) and non-singular

or at most weakly-singular integral equations. The generality is given by the possibility of employing the method to problems with arbitrary continuous variation of the material coefficients. On the other hand, the employed finite-element mesh can be successfully utilized for the post-processing of numerical results. Recall that a physically acceptable solution approach to a structural-field problem in a continuum theory is subject to two principle demands: (i) incorporation of complete boundary conditions, (ii) involvement of the whole bulk of material into the interaction, *i.e.*, full information on the whole boundary as well as the domain should be incorporated into the numerical approach. Both these requirements are satisfied in a natural and reasonable way by discretizing the whole structure into finite-size domain elements and numerical simulation of the field variable within such elements by a polynomial interpolation. As compared with the weak formulations used in the standard FEM, the present approach is based on the numerical solution of the exact integro-differential equations by using the same polynomial approximation within the domain elements. The resulting system matrix is sparse as in the standard FEM. As compared with the boundary-domain formulation, no regularization procedure is required, since the employed integro-differential equations are either non-singular or at most weakly singular. Moreover, the inconsistency in the approximation concept is removed.

Several test examples are presented to verify the proposed method.

2. Integral-equation formulation for potential problems in non-homogeneous materials

Let us consider the potential problem in non-homogeneous materials [30, Chapter 3]. The governing equation is given by

$$(k(\mathbf{x})u_{,i}(\mathbf{x}))_{,i} = f(\mathbf{x}) \text{ in } \Omega. \tag{1}$$

Among many physical interpretations, $u(\mathbf{x})$ could be regarded as the stationary temperature field with k and f being the heat-conduction coefficient and the body heat-source density, respectively. The subscripts following a comma denote partial derivatives with respect to Cartesian coordinates.

Assuming $k(\mathbf{x})$ to be a differentiable function of the spatial coordinates and non-vanishing in Ω, Equation (1) can be rearranged as

$$\nabla^2 u(\mathbf{x}) + \frac{k_{,i}(\mathbf{x})}{k(\mathbf{x})} u_{,i}(\mathbf{x}) = \frac{f(\mathbf{x})}{k(\mathbf{x})}. \tag{2}$$

For simplicity, let us consider the Dirichlet and the Neumann boundary conditions given by

$$\begin{aligned} &u(\boldsymbol{\eta}) = \bar{u}(\boldsymbol{\eta}) \quad \text{if } \boldsymbol{\eta} \in \partial\Omega_D, \\ &\frac{\partial u}{\partial n}(\boldsymbol{\eta}) = \frac{\bar{q}(\boldsymbol{\eta})}{k(\boldsymbol{\eta})} \quad \text{if } \boldsymbol{\eta} \in \partial\Omega_N, \end{aligned} \tag{3}$$

where $\partial\Omega = \partial\Omega_D \cup \partial\Omega_N$ is the complete boundary of the domain Ω.
Strictly speaking, the flux $\bar{q}$ is prescribed on $\partial\Omega_N$. However, the normal derivative is related to the flux $\bar{q}$ by $\partial u/\partial n = \bar{q}/k$.

It should be remarked that the fundamental solution for the differential operator

$$\left(\nabla^2 + \frac{k_{,i}(\mathbf{x})}{k(\mathbf{x})}\partial_i\right)$$

cannot, in general, be given in closed form, except for special cases [9–15]. Nevertheless, one can formulate the solution of the above-stated BVP using the boundary-domain-integral-equation approach [7]. For this purpose, one can use the fundamental solution of the Laplace

operator which is defined as the solution of Poisson's equation in an infinite space with a point source, *i.e.*,

$$\nabla^2 G(|\mathbf{x}-\mathbf{y}|) = -\delta(\mathbf{x}-\mathbf{y}), \tag{4}$$

where $\delta(\mathbf{r})$ is the Dirac δ-function. It is well known that

$$G(r) = \begin{cases} -\dfrac{1}{2\pi}\log\left(\dfrac{r}{r_o}\right), & \text{for } 2d \text{ problems} \\ \dfrac{1}{4\pi r}, & \text{for } 3d \text{ problems} \end{cases} \tag{5}$$

in which $r = |x-y|$ and r_o is an arbitrary constant used for getting a non-dimensional argument for the logarithmic function.

Making use of the fundamental solution of the Laplace operator, we can recast the integral identity

$$\int_\Omega G(|\mathbf{x}-\mathbf{y}|)\,\nabla^2 u(\mathbf{x})\mathrm{d}\Omega(\mathbf{x}) = \int_\Omega \frac{G(|\mathbf{x}-\mathbf{y}|)}{k(\mathbf{x})}\left[f(\mathbf{x}) - k_{,j}(\mathbf{x})u_{,j}(\mathbf{x})\right]\mathrm{d}\Omega(\mathbf{x}) \tag{6}$$

into an integral representation for the potential field

$$\begin{aligned} c(\mathbf{y})u(\mathbf{y}) = &\int_{\partial\Omega}\left[\frac{\partial u}{\partial n}(\boldsymbol{\eta})G(|\boldsymbol{\eta}-\mathbf{y}|) - u(\boldsymbol{\eta})\frac{\partial G(|\boldsymbol{\eta}-\mathbf{y}|)}{\partial n(\boldsymbol{\eta})}\right]\mathrm{d}\Gamma(\boldsymbol{\eta}) \\ &- \int_\Omega \frac{G(|\mathbf{x}-\mathbf{y}|)}{k(\mathbf{x})}\left[f(\mathbf{x}) - k_{,j}(\mathbf{x})u_{,j}(\mathbf{x})\right]\mathrm{d}\Omega(\mathbf{x}), \end{aligned} \tag{7}$$

with

$$c(\mathbf{y}) = \begin{cases} 1, & \mathbf{y}\in\Omega \\ 0, & \mathbf{y}\notin(\Omega\cup\partial\Omega). \end{cases} \tag{8}$$

Note that all the integrals exist in the normal sense as long as the source point $\mathbf{y}$ does not lie on the boundary $\partial\Omega$. The limit case $\mathbf{y}\to\zeta\in\partial\Omega$ will be considered later in Equation (24) where all the integrals still exist in a normal sense.

Owing to the domain integral containing the unknown potential gradients, Equation (7) no longer has the character of a pure boundary-integral formulation. Thus, it is insufficient to solve the system of boundary-integral equations (BIEs) for the boundary unknowns: one has to discretize the interior of the domain also in order to compute simultaneously the potential gradients. The integral representation for the potential gradients can be obtained directly by differentiating Equation (7), either without regularization, which leads to a hypersingular integral representation, or with a subsequent regularization, which results in a non-hypersingular integral representation with strongly singular kernels [7]. In such a boundary-domain formulation, the boundary unknowns are approximated independently as in the standard BEM formulation and the potential gradients in the interior are expressed in terms of the potential at interior nodes by using the finite-element approximation within interior cells. Note that these two types of approximation are inherently inconsistent. In the following sections, we propose another method based on a finite-element approximation throughout the domain Ω and use of local integral equations for coupling the nodal values.

3. Domain-element approximation

Contrary to the pure BEM, the dimensionality of the problem is not reduced if domain integrals are involved. It should be pointed out that by approximating a field within a domain element, one can get the gradients of that field by differentiating the approximation of the primary field. Thus, the concept of independent approximations of boundary densities employed in the discretization of the BIEs is not consistent with the concept of domain-type approximation of the same primary field as proposed in the boundary-domain formulation of the integral-equation approach.

Let us consider a 2-D plane domain Ω to be subdivided into m conforming quadrilateral serendipity elements $S_e, e=1,\dots,m$, by using polynomial interpolation for the approximation of both the geometry and the potential field. Then,

$$\Omega = \bigcup_{e=1}^{m} S_e, \qquad u(\mathbf{x})|_{S_e} = \sum_{a=1}^{n} u(\mathbf{x}^{ae}) N^a(\xi_1,\xi_2), \qquad x_i|_{S_e} = \sum_{a=1}^{n} x_i^{ae} N^a(\xi_1,\xi_2), \tag{9}$$

where x_i^{ae} are the Cartesian coordinates of the a-th nodal point on S_e, and N^a represent the shape functions. On each domain element, one can define two non-collinear vectors $\mathbf{h}_\alpha^e(\xi_1,\xi_2)$ for $\alpha=1,2$ with the Cartesian components

$$h_{\alpha i}^e(\xi_1,\xi_2) = \sum_{a=1}^{n} x_i^{ae} \frac{\partial N^a(\xi_1,\xi_2)}{\partial \xi_\alpha}, \quad (i=1,2). \tag{10}$$

The Cartesian components of the gradients of the approximated field are expressed in terms of the partial derivatives with respect to the intrinsic coordinates by using the transformation relationship

$$\left.\frac{\partial(g)}{\partial x_i}\right|_{S_e} = \frac{\partial \xi_j}{\partial x_i}\left.\frac{\partial(g)}{\partial \xi_j}\right|_{S_e} = \left(\mathbf{h}^e\right)_{ij}^{-1}\left.\frac{\partial(g)}{\partial \xi_j}\right|_{S_e} \tag{11}$$

where $(\mathbf{h}^e)^{-1}$ is the inverse matrix to the matrix $\mathbf{h}^e$ defined by (10). Since

$$\left(\mathbf{h}^e\right)_{ij}^{-1} = \frac{\varepsilon_{3il}\varepsilon_{3jk} h_{kl}^e(\xi_1,\xi_2)}{\varepsilon_{3mn} h_{1m}^e(\xi_1,\xi_2) h_{2n}^e(\xi_1,\xi_2)} \tag{12}$$

we may write

$$\left.\frac{\partial u(\mathbf{x})}{\partial x_i}\right|_{S_e} = \frac{\varepsilon_{3il}\varepsilon_{3jk} h_{kl}^e(\xi_1,\xi_2)}{\varepsilon_{3mn} h_{1m}^e(\xi_1,\xi_2) h_{2n}^e(xi_1,\xi_2)} \sum_{a=1}^{n} u(\mathbf{x}^{ae}) \frac{\partial N^a(\xi_1,\xi_2)}{\partial \xi_j}, \tag{13}$$

where ε_{kij} is the permutation tensor, $\varepsilon_{312} = -\varepsilon_{321} = 1, \varepsilon_{311} = \varepsilon_{322} = 0$. Hence, one can also express the normal derivatives of the potential on the boundary of the domain in terms of nodal values of the potential field. Thus, collocating the Dirichlet and the Neumann boundary conditions, we obtain a subsystem of linear algebraic equations for the computation of the potential values at all nodal points

$$u^b = \bar{u}(\zeta^b), \qquad \text{if } \zeta^b \in \partial\Omega_D \tag{14}$$

$$\frac{n_i(\zeta^b)}{m^b} \sum_{S_e \ni \zeta^b} \left(\mathbf{h}^e\right)_{ij}^{-1}\left(\xi_1^{be},\xi_2^{be}\right) \sum_{a=1}^{n} u(\mathbf{x}^{ae}) \frac{\partial N^a}{\partial \xi_j}\left(\xi_1^{be},\xi_2^{be}\right)$$

$$= \frac{\bar{q}(\zeta^b)}{k(\zeta^b)}, \qquad \text{if } \zeta^b \in (\partial\Omega_N - \partial\Omega_D), \tag{15}$$

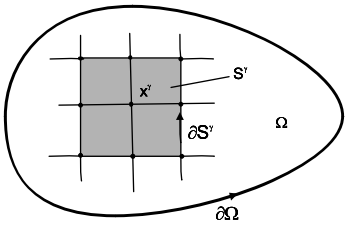

Figure 1. Illustration of the sub-domain S^γ and its boundary ∂S^γ.

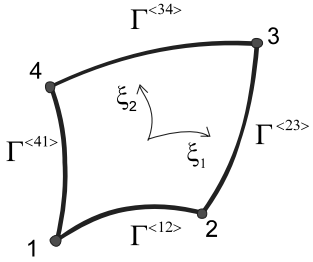

Figure 2. A quadrilateral element with its corner nodes and boundary sides $\Gamma^{\langle fp \rangle}$.

in which (ξ_1^{be}, ξ_2^{be}) are the intrinsic coordinates of $\zeta^b \in S_e$; m^b is the number of discretization elements adjacent to ζ^b. The unit normal vector $n_i(\zeta^b)$ is taken as the average of normal vectors evaluated at ζ^b if $m^b > 1$. Assuming existence of potential gradients at corners, one can select arbitrarily one of two sides joined at the corner for the definition of the normal vector $n_i(\zeta^b)$ and the prescribed flux $\bar{q}(\zeta^b)$ in (15), provided that the Neumann boundary conditions are prescribed on both sides of the corner.

Bearing in mind the present concept of approximating field unknowns in terms of potential values, it is more appropriate to regard (7) as the integro-differential representation of the potential field, since both the integral and the differential operators are applied on the unknown field.

The shape functions and their derivatives for the bi-linear, quadratic, cubic and quartic quadrilateral Lagrange elements are given in the Appendix. The rest of the system of linear algebraic equations will be obtained by discretization of the local integro-differential representations of the potential field at interior nodes.

4. Local integro-differential equations

Recall that all the considerations given in Section 2 are valid for any sub-domain of the whole body Ω. Let S^γ denote the union of all domain elements S_e adjacent to the interior nodal point $\mathbf{x}^\gamma$ (see Figure 1), with S_e being assumed to be closed. Thus,

$$S^\gamma = \bigcup_{\substack{e=1 \\ x^\gamma \in S_e}}^{m} S_e, \quad \text{with } \Omega = \bigcup_{e=1}^{m} S_e. \tag{16}$$

According to Equation (7), we may write the local integro-differential representation of the potential at $\mathbf{x}^\gamma$ in terms of the potential and its normal derivative on the boundary ∂S^γ, as well as the potential gradients in S^γ, as

$$u(\mathbf{x}^\gamma) = \int_{\partial S^\gamma} \left[\frac{\partial u}{\partial n}(\boldsymbol{\eta}) G\left(|\boldsymbol{\eta} - \mathbf{x}^\gamma|\right) - u(\boldsymbol{\eta}) \frac{\partial G\left(|\boldsymbol{\eta} - \mathbf{x}^\gamma|\right)}{\partial n(\boldsymbol{\eta})} \right] \mathrm{d}\Gamma(\boldsymbol{\eta}) - \int_{S^\gamma} \frac{G\left(|\mathbf{x} - \mathbf{x}^\gamma|\right)}{k(\mathbf{x})} \left[f(\mathbf{x}) - k_{,j}(\mathbf{x}) u_{,j}(\mathbf{x}) \right] \mathrm{d}\Omega(\mathbf{x}). \tag{17}$$

In view of the conforming element approximation, the discretized form of the local integro-differential Equation (17) is given as

$$u(\mathbf{x}^{\gamma}) = \sum_{S_e \ni \mathbf{x}^{\gamma}} \sum_{a=1}^{n} u(\mathbf{x}^{ae}) \times \left\{ \sum_{\langle fp \rangle}^{'c_e} \int_{-1}^{1} n_i^{e\langle fp \rangle}(s) \left[(\mathbf{h}^e)_{ij}^{-1} \left(\xi_1^{\langle fp \rangle}, \xi_2^{\langle fp \rangle} \right) \frac{\partial N^a}{\partial \xi_j} \left(\xi_1^{\langle fp \rangle}, \xi_2^{\langle fp \rangle} \right) G(|\boldsymbol{\eta}^{e\langle fp \rangle} - \mathbf{x}^{\gamma}|) \right.\right.$$
$$\left. - N^a \left(\xi_1^{\langle fp \rangle}, \xi_2^{\langle fp \rangle} \right) G_{,i}(|\boldsymbol{\eta}^{e\langle fp \rangle} - \mathbf{x}^{\gamma}|) \right] \tau^{e\langle fp \rangle}(s) \mathrm{d}s + \int_{-1}^{1} \int_{-1}^{1} \frac{G(|\mathbf{x}(\xi) - \mathbf{x}^{\gamma}|)}{k(\mathbf{x}(\xi))}$$
$$\left. \times \left[k_{,i}(\mathbf{x}(\xi)) (\mathbf{h}^e)_{ij}^{-1}(\xi_1, \xi_2) \frac{\partial N^a(\xi_1, \xi_2)}{\partial \xi_j} - f(\mathbf{x}(\xi)) \right] J^e(\xi_1, \xi_2) \mathrm{d}\xi_1 \mathrm{d}\xi_2 \right\}, \tag{18}$$

in which c_e is the local number of collocation points on the finite element S_e (*i.e.*, $\mathbf{x}^{\gamma} = \mathbf{x}^{c_e}$), and the boundary contour ∂S^{γ} is decomposed into finite portions defined by the element sides $\Gamma_{\mathrm{e}}^{\langle fp \rangle}$ as

$$\partial S^{\gamma} = \sum_{S_e \ni \mathbf{x}^{\gamma}} \bigcup_{\langle fp \rangle}^{'c_e} \Gamma_{\mathrm{e}}^{\langle fp \rangle} \quad \text{with} \quad \langle fp \rangle \in \{\langle 12 \rangle, \langle 23 \rangle, \langle 34 \rangle, \langle 41 \rangle\} \tag{19}$$

and $\bigcup_{\langle fp \rangle}^{'c_e} (\bullet) = \bigcup_{\substack{\langle fp \rangle \\ x^{ce} \notin \Gamma_{\mathrm{e}}^{\langle fp \rangle}}} (\bullet)$, $\sum_{\langle fp \rangle}^{'c_e} (\bullet) \equiv \sum_{\substack{\langle fp \rangle \\ x^{ce} \notin \Gamma_{\mathrm{e}}^{\langle fp \rangle}}} (\bullet)$.

The notation $\Gamma_{\mathrm{e}}^{\langle fp \rangle}$ is used for that side of the quadrilateral element S_e which lies between the local nodes f and p as shown in Figure 2.
The intrinsic coordinates $\left(\xi_1^{\langle fp \rangle}, \xi_2^{\langle fp \rangle}\right)$ and the tangent vector $\tau_i^{e\langle fp \rangle}$ on $\Gamma_{\mathrm{e}}^{\langle fp \rangle} \subset S_e$ are defined as follows

$$\begin{aligned}
&\xi_1^{\langle 12 \rangle} = s, \xi_2^{\langle 12 \rangle} = -1, && \tau_i^{e\langle 12 \rangle}(s) = h_{1i}^e(s, -1), \\
&\xi_1^{\langle 23 \rangle} = 1, \xi_2^{\langle 23 \rangle} = s, && \tau_i^{e\langle 23 \rangle}(s) = h_{2i}^e(1, s), \\
&\xi_1^{\langle 34 \rangle} = s, \xi_2^{\langle 34 \rangle} = 1, && \tau_i^{e\langle 34 \rangle}(s) = -h_{1i}^e(s, 1), \\
&\xi_1^{\langle 41 \rangle} = -1, \xi_2^{\langle 41 \rangle} = s, && \tau_i^{e\langle 41 \rangle}(s) = -h_{2i}^e(-1, s),
\end{aligned} \tag{20}$$

with $s \in [-1, 1]$. Then, the global Cartesian coordinates of the field point, the unit normal vector and the Jacobian of the transformation from the global coordinates to the intrinsic ones on $\Gamma_{\mathrm{e}}^{\langle fp \rangle} \subset S_e$ are given as

$$\eta_k^{e\langle fp \rangle} = \sum_{a=1}^{n} x_k^{ae} N^a \left(\xi_1^{\langle fp \rangle}, \xi_2^{\langle fp \rangle} \right), \qquad n_i^{e\langle fp \rangle}(s) = \varepsilon_{ij3} \tau_j^{e\langle fp \rangle}(s) / \tau^{e\langle fp \rangle}(s),$$
$$\tau^{e\langle fp \rangle}(s) = \sqrt{\tau_j^{e\langle fp \rangle}(s) \tau_j^{e\langle fp \rangle}(s)}. \tag{21}$$

The Cartesian coordinates of the integration points on S_e are given as

$$x_k|_{S_e} = \sum_{a=1}^{n} x_k^{ae} N^a(\xi_1, \xi_2), \quad \xi_1, \xi_2 \in [-1, 1] \tag{22}$$

and $J^e(\xi_1, \xi_2)$ is the Jacobian of the transformation $(x_1, x_2) \to (\xi_1, \xi_2)$ which is given by

$$J^e(\xi_1, \xi_2) = \left| \varepsilon_{3ij} h_{1i}^e(\xi_1, \xi_2) h_{2j}^e(\xi_1, \xi_2) \right|. \tag{23}$$

It is convenient to employ the polar coordinate system in the intrinsic space with the centre at (ξ_1^c, ξ_2^c) corresponding to the collocation point $\mathbf{x}^{c_e}$ in order to eliminate the logarithmic singularity in the domain integral. Although the contour integrations and the integration with respect to the radial variable can be performed analytically in the case of bilinear Lagrange elements, the numerical integrations by standard Gauss-Legendre quadrature yield very accurate results.

Equations (14), (15) and (18) form a complete set of linear algebraic equations for the computation of the nodal values of the potential. Because of the local character of these equations, the system matrix is sparse as in standard FEM.

As an alternative to Equation (15), one can also use the LIDE collocated at the boundary nodes on the Neumann part of the boundary. A suitable form of that LIDE is given as follows

$$\int_{\partial S^b} \left\{ \left[u(\boldsymbol{\eta}) - u(\zeta^b) \right] \frac{\partial G\left(\left|\boldsymbol{\eta} - \zeta^b\right|\right)}{\partial n(\boldsymbol{\eta})} - \frac{\partial u}{\partial n}(\boldsymbol{\eta}) G\left(\left|\boldsymbol{\eta} - \zeta^b\right|\right) \right\} \mathrm{d}\Gamma(\boldsymbol{\eta})$$
$$- \int_{S^b} u_{,j}(\mathbf{x}) \frac{k_{,j}(\mathbf{x})}{k(\mathbf{x})} G\left(\left|\mathbf{x} - \zeta^b\right|\right) d\Omega(\mathbf{x}) = - \int_{S^b} \frac{f(\mathbf{x})}{k(\mathbf{x})} G\left(\left|\mathbf{x} - \zeta^b\right|\right) \mathrm{d}\Omega(\mathbf{x}), \quad \zeta^b \in \partial\Omega_N, \tag{24}$$

where the subdomain S^b is defined by (16) as the union of domain elements adjacent to the boundary collocation point ζ^b. Recall that the local boundary ∂S^b is composed of both the non-singular and singular sides of the finite elements adjacent to ζ^b. The former lie in the interior of Ω, while the singular sides lie on the global boundary $\partial\Omega$) ζ^b (more precisely, on its Neumann part $\partial\Omega_N \subset \partial\Omega$). In the illustrative Figure 3, the singular sides are $\partial S_{e_1} \cap \partial\Omega$ and $\partial S_{e_2} \cap \partial\Omega$ when $S^b = S_{e_1} \cup S_{e_2}$, while one singular side $\partial S_e \cap \partial\Omega$ takes place when the sub-domain S^b is formed by one domain element $S^b = S_e$.

The integration over those $\Gamma_e^{\langle fp \rangle}$, which do not lie on the global boundary $\partial\Omega$, is the same as in the case of the LIDE collocated at an interior node. One should be careful when integrating over $\Gamma_e^{\langle fp \rangle} \subset \partial\Omega_N \subset \partial\Omega$, because the collocation point ζ^b lies on those $\Gamma_e^{\langle fp \rangle}$ too. To illustrate this, let us consider the integration over $\Gamma_e^{\langle 23 \rangle}$ with $\mathbf{x}^{2e}, \mathbf{x}^{3e} \in \partial\Omega$. If we use the quadratic approximation, the Taylor series expansion of the shape function $N^a(\xi_1, \xi_2)$ on $\Gamma_e^{\langle 23 \rangle}$ is given as

$$N^a(1, s) = N^a\left(1, \xi_2^b\right) + \sum_{k=1}^{2} \frac{1}{k!} \left(s - \xi_2^b\right)^k \frac{\partial^k N^a}{\partial \xi_2^k}\left(1, \xi_2^b\right), \quad \xi_2 = s \in [-1, 1].$$

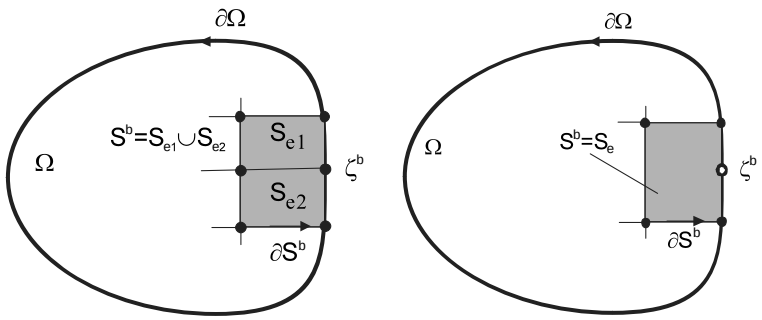

Figure 3. Illustration of two possibilities for the sub-domain S^b (and its boundary ∂S^b) created by either two or one quadrilateral discretization elements adjacent to the boundary node ζ^b.

Hence,

$$r_i|_{\Gamma_{23}} = \left(\eta_i - \zeta_i^b\right)\Big|_{\Gamma_e^{\langle 23\rangle}} = \left(s - \xi_2^b\right) R_i^{eb}(s), \quad R_i^{eb}(s)$$
$$\equiv \sum_{a=1}^{8} x_i^{ae}\left[\frac{\partial N^a}{\partial \xi_2}\left(1, \xi_2^b\right) + \frac{\left(s - \xi_2^b\right)}{2}\frac{\partial^2 N^a}{\partial \xi_2^2}\left(1, \xi_2^b\right)\right], \tag{25}$$
$$\left[u(\eta) - u\left(\zeta^b\right)\right]\Big|_{\Gamma_e^{\langle 23\rangle}} = \left(s - \xi_2^b\right)\sum_{a=1}^{8} u\left(\mathbf{x}^{ae}\right)\left[\frac{\partial N^a}{\partial \xi_2}\left(1, \xi_2^b\right) + \frac{\left(s - \xi_2^b\right)}{2}\frac{\partial^2 N^a}{\partial \xi_2^2}(1, \xi_2^b)\right]$$

and finally, in view of Equations (20), (21) and (25), we have

$$\int_{\Gamma_e^{\langle 23\rangle}} \left[u(\eta) - u(\zeta^b)\right]\frac{\partial G}{\partial n}(\eta - \zeta^b)\tau(\eta)\mathrm{d}\Gamma(\eta)$$
$$= -\frac{\varepsilon_{ij3}}{2\pi}\sum_{a=1}^{8} u(\mathbf{x}^{ae})\int_{-1}^{1}\frac{h_{2j}(1,s)R_i^{eb}(s)}{\left(R^{eb}(s)\right)^2}\left[\frac{\partial N^a}{\partial \xi_2}(1, \xi_2^b) + \frac{(s - \xi_2^b)}{2}\frac{\partial^2 N^a}{\partial \xi_2^2}(1, \xi_2^b)\right]\mathrm{d}s \tag{26}$$

with $R^{eb} = \sqrt{R_i^{eb} R_i^{eb}}$ being bounded within the whole interval $s \in [-1, 1]$. Thus, the integrand involving the normal derivative of the fundamental solution is bounded on $\Gamma_e^{\langle 23\rangle}$.

As to the other boundary integral in (24), it becomes on $\Gamma_e^{\langle 23\rangle}$

$$\int_{\Gamma_e^{\langle 23\rangle}} \frac{\partial u}{\partial n}(\eta) G\left(\left|\eta - \zeta^b\right|\right) d\Gamma(\eta) = \int_{\Gamma_e^{\langle 23\rangle}} \frac{\bar{q}(\eta)}{k(\eta)} G\left(\left|\eta - \zeta^b\right|\right)\mathrm{d}\Gamma(\eta), \tag{27}$$

where $\bar{q}(\eta)$ is either expressed as a given function at each point on $\Gamma_e^{\langle 23\rangle}$ (with $\eta_i\big|_{\Gamma_e^{\langle 23\rangle}} = (s - \xi_2^b)R_i^{eb} + \zeta_i^b$) or its variation is approximated over the prescribed nodal values on $\Gamma_e^{\langle 23\rangle}$ as

$$\bar{q}(\eta)|_{\Gamma_e^{\langle 23\rangle}} = \sum_{a=1}^{8} \bar{q}^{ae} N^a(1, s),$$

where the shape functions $N^a(1, s)$ vanish, if the a-th nodal point does not lie on $\Gamma_e^{\langle 23\rangle}$. Thus, the integral (27) becomes

$$\int_{\Gamma_e^{\langle 23\rangle}} \frac{\bar{q}(\eta)}{k(\eta)} G(\left|\eta - \zeta^b\right|)\mathrm{d}\Gamma(\eta)$$
$$= -\frac{1}{2\pi}\int_{-1}^{1}\frac{\bar{q}(\eta(s))}{k(\eta(s))}\left[\log\left(\left|s - \xi_2^b\right|\right) + \log\left(\frac{R^{eb}(s)}{r_o}\right)\right]\tau(s)\mathrm{d}s \tag{28a}$$

or

$$\int_{\Gamma_e^{\langle 23\rangle}} \frac{\bar{q}(\eta)}{k(\eta)} G(\left|\eta - \zeta^b\right|)\mathrm{d}\Gamma(\eta)$$
$$= -\frac{1}{2\pi}\sum_{a=1}^{8}\bar{q}^{ae}\int_{-1}^{1}\frac{N^a(1,s)}{k(\eta(s))}\left[\log\left(\left|s - \xi_2^b\right|\right) + \log\left(\frac{R^{eb}(s)}{r_o}\right)\right]\tau(s)\mathrm{d}s, \tag{28b}$$

respectively, according to the two kinds of prescribed data for the flux on $\Gamma_e^{\langle 23\rangle}$. Recall that $\tau(s) = \left(h_{2j}(1,s)h_{2j}(1,s)\right)^{1/2}$ and the extracted logarithmic singular term can be integrated by using a special logarithmic Gauss quadrature. All the other integrals can be integrated by regular Gauss-Legendre quadrature.

5. Numerical experiments

In order to test the proposed method, we consider some examples for which the analytical solution is available and can be used as a benchmark solution. In all cases, we consider a 2-D potential problem with the governing equation given as

$$\nabla^2 u(\mathbf{x}) + \frac{k_{,i}(\mathbf{x})}{k(\mathbf{x})} u_{,i}(\mathbf{x}) = 0 \text{ in } \Omega, \tag{29}$$

in which the continuously variable coefficient $k(\mathbf{x}) \neq 0$. In the literature, the spatial variation of material coefficients for FGMs is usually assumed as exponential or of power-law type. In the present paper, we merely test the proposed numerical method without any relation to concrete materials. In all numerical computations, we have used conforming quadrilateral serendipity elements and the numerical integrations have been carried out by regular Gauss-Legendre quadrature with 12 integration points.

5.1. Example 1

Let us consider the BVP governed by Equation (29) in a square $L \times L$ with the exponentially graded material coefficient in the x_2-direction being given by

$$k(\mathbf{x}) = k_o \mathrm{e}^{\delta x_2 / L}, \tag{30}$$

where δ is a dimensionless material parameter. The boundary conditions are given as follows

$$\begin{aligned} &u(\mathbf{x}) = u_o \text{ for } x_1 \in [0, L] \wedge x_2 = 0, \quad u(\mathbf{x}) = u_L \text{ for } x_1 \in [0, L] \wedge x_2 = L, \\ &q(\mathbf{x}) = 0 \text{ for } x_1 = 0 \text{ or } L \wedge x_2 \in [0, L]. \end{aligned} \tag{31}$$

The exact solution of this 1-D problem is given by

$$u(\mathbf{x}) = u_o + [u_L - u_o] \frac{1 - \mathrm{e}^{-\delta x_2 / L}}{1 - \mathrm{e}^{-\delta}}. \tag{32}$$

5.1.1. *Convergence study*

In order to compare the accuracy of the numerical calculations for various discretization meshes, we have evaluated the global % error defined by L_2 norm error

$$\mathrm{GPE} = 100 \left\{ \int_\Omega \left[u^c(\mathbf{x}) - u^{ex}(\mathbf{x}) \right]^2 \mathrm{d}\Omega(x) \right\}^{1/2} \Bigg/ \left\{ \int_\Omega \left[u^{ex}(\mathbf{x}) \right]^2 \mathrm{d}\Omega(x) \right\}^{1/2}, \tag{33}$$

We present the results of the investigation based on the use of:

(i) two different material media characterized by $\delta \in \{0, 2\}$;
(ii) four different orders of serendipity elements (linear, quadratic, cubic, quartic);
(iii) two kinds of discretization meshes:
   (a) non-uniform meshes based on splitting the square sample width into two elements and the height into $m/2$ elements with $m = 4, 8, 10$, and 20 domain elements (the corresponding total numbers of nodes are given in Table 1)
   (b) uniform meshes with homogeneous distribution of nodal points in both the x_1 and x_2 directions with $m = 4, 9, 16, 25, 64, 100$ square elements.

Table 1. The total numbers of nodal points corresponding to the employed orders of approximation.

Number of elements m	Linear	Quadratic	Cubic	Quartic
$m=4$	9	21	33	45
$m=8$	15	37	59	81
$m=10$	18	45	72	99
$m=20$	33	85	137	189

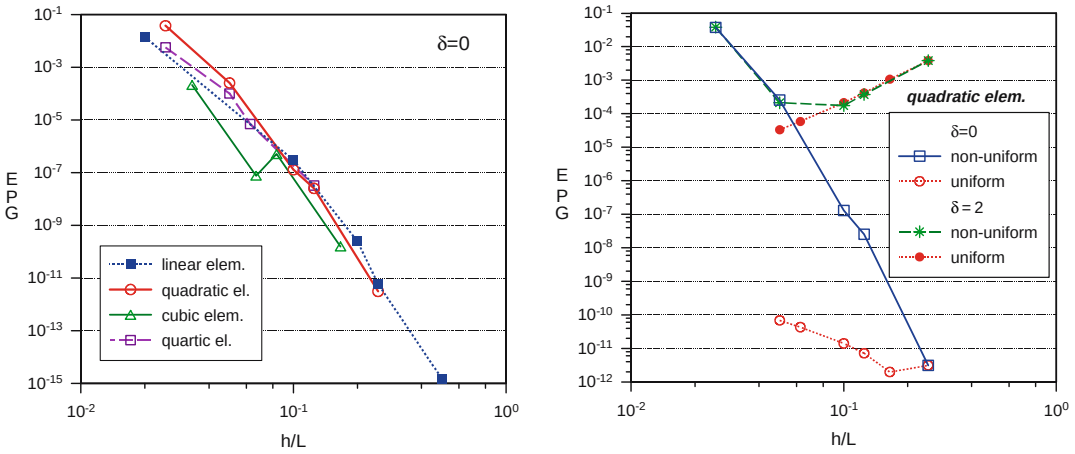

Figure 4. The dependence of the global % error on the dimensionless mesh parameter for: (i) the homogeneous medium ($\delta=0$) using four different kinds of quadrilateral elements. (ii) two different media ($\delta=0$, $\delta=2$) using two different kinds of meshes of quadratic elements.

In order to compare the numerical results obtained by using various discretization meshes, we shall use the shortest distance between any two nodal points h as a mesh characteristic.

The increase of the number of discretization elements and/or their order can improve the approximation of both the geometrical and field variables by interpolation within the element in some problems. On the hand, the increase of the number of nodal points (nodal unknowns) gives rise to calculation errors. In the analysed simple problem in a homogeneous medium, the exact solution is linearly dependent on the x_2-coordinate. The integration along straight lines is exact and the domain integrals are not involved. Thus, any increase of nodal points is not expected to improve the accuracy as compared with that achieved by using the coarsest mesh of linear elements. This expectation is confirmed by Figure 4. Since the solution is independent of the x_1-coordinate, it is natural to make the discretization finer in the x_2 direction, as assumed in the employed non-uniform meshes. Such a discretization, however, leads to flattened-out elements what is finally the other source of computational errors. From Figure 4 for a non-homogeneous medium, one can see the improvement of the accuracy when decreasing the dimensionless parameter h/L and when a uniform mesh of square elements is used. This is the influence of the improvement of the approximation accuracy for the potential field and its gradients by increasing the number of elements. A similar trend can also be seen in the case of non-uniform meshes in the initial stage of mesh refining, but a further flattening-out of the elements yields a final decrease of the accuracy. Finally, this negative influence becomes dominant for dense meshes and the accuracy is the same as in the case of a homogeneous medium ($\delta=0$). For a homogeneous medium, a global decrease of the accuracy is

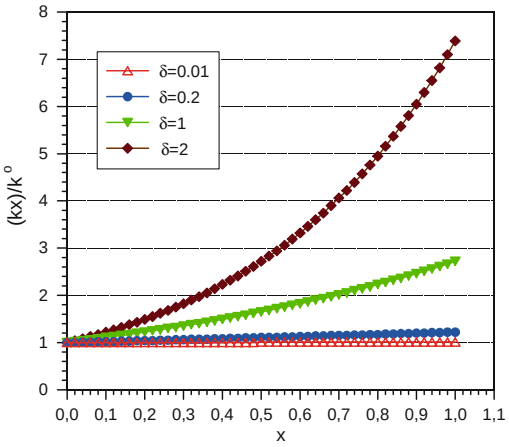

Figure 5. Variation of the dimensionless material coefficient within the sample thickness $x = x_2/L$ for the case of exponential gradation.

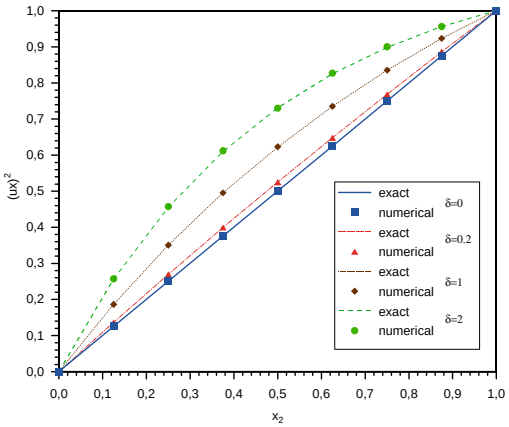

Figure 6. Potential field in a square along the direction of variation of material coefficient with exponential gradation.

observed when h/L is decreased, even in the case of uniform meshes, as can be seen from Figure 4.

In what follows, we shall present the numerical results obtained by using the quadrilateral conforming elements with quadratic approximation.

5.1.2. *Visualization of numerical and analytical results*

As an illustration, we present the variation of the material coefficient in the direction of the non-homogeneity for four different values of the material parameter δ. It can be seen from Figure 5 that the enhancement of the material coefficient on the top of the square sample is remarkable for $\delta = 2$ and also for $\delta = 1$. Nevertheless, the numerical solution perfectly fits the exact one for each considered value of the material parameter δ, as is seen from Figure 6. The results have been obtained by using a non-uniform mesh with eight elements.

5.2. Example 2

In this example, the geometry and boundary conditions are the same as in Example 1. The only difference is in the variation of the material coefficient which is now given by the power law

$$k(\mathbf{x}) = (1 + \delta x_2/L)^n. \tag{34}$$

The considered BVP is again 1-D and one can easily find the exact solution, which is

$$u(\mathbf{x}) = u_o + [u_L - u_o]\frac{\log(1+\delta x_2/L)}{\log(1+\delta)} \quad \text{for } n = 1,$$
$$u(\mathbf{x}) = u_o + [u_L - u_o]\frac{(1+\delta x_2/L)^{1-n} - 1}{(1+\delta)^{1-n} - 1} \quad \text{for } n \neq 1. \tag{35}$$

We present the numerical results for the exponent $n = 2$. The material coefficient variation is similar as in Example 1, but its relative increase at the top of the sample is higher (see Figure 7).

The computed values of the potential field again fit perfectly the analytical values (Figure 8). A slightly worse accuracy is obtained for the case of the material

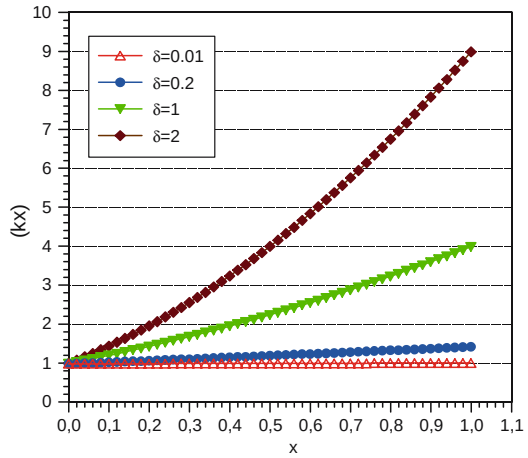

Figure 7. Variation of the material coefficient within the sample thickness $x = x_2/L$ for the case of power-law gradation.

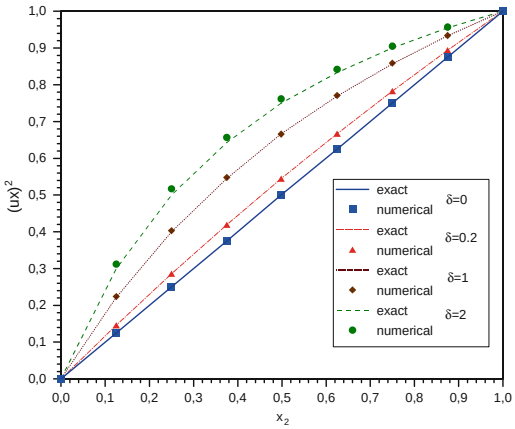

Figure 8. Potential field in a square along the direction of variation of material coefficient with power-law gradation.

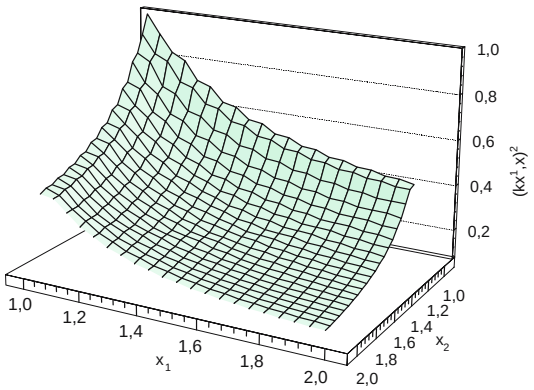

Figure 9. The spatial variation of the material coefficient.

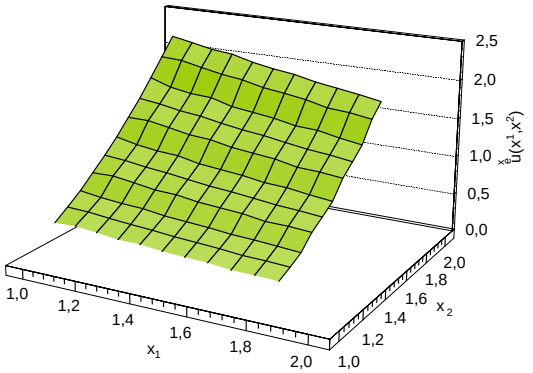

Figure 10. The surface of the exact solution of the BVP.

parameter $\delta = 2$, when the global percentage error is 0.6932% by using a non-uniform mesh with eight elements.

5.3. Example 3

As a further demonstration of the accuracy of the method, we consider the BVP governed by Equation (29) in a square $[1, 2] \times [1, 2]$ with the material coefficient graded in two directions as

$$k(\mathbf{x}) = \left(\frac{1}{x_1 x_2}\right)^2. \tag{36}$$

The analytical solution [14] is

$$u(\mathbf{x}) = \frac{1}{2}(x_2^2 - x_1^2)\tan^{-1}\left(\frac{x_2}{x_1}\right) + \frac{x_1 x_2}{2}. \tag{37}$$

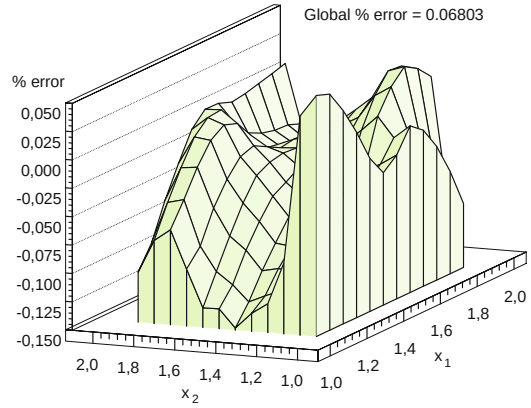

Figure 11. The global % error and the distribution of the % error within the sample discretized into 10 uniform quadratic elements.

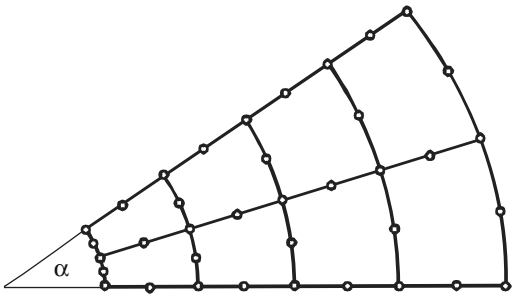

Figure 12. Discretization mesh for the tube section with 8 quadrilateral quadratic elements.

It obeys the boundary conditions

$$u(x_1,1)=\frac{1}{2}(1-x_1^2)\tan^{-1}\left(\frac{1}{x_1}\right)+\frac{x_1}{2},\qquad u(x_1,2)=\frac{1}{2}(4-x_1^2)\tan^{-1}\left(\frac{2}{x_1}\right)+x_1,$$
$$q(1,x_2)=-k(1,x_2)u_{,1}(1,x_2),\qquad q(2,x_2)=k(2,x_2)u_{,1}(2,x_2), \tag{38}$$

with the potential gradients being given as

$$u_{,1}(\mathbf{x})=-x_1\tan^{-1}\left(\frac{x_2}{x_1}\right)+\frac{x_1^2x_2}{x_1^2+x_2^2},\qquad u_{,2}(\mathbf{x})=x_2\tan^{-1}\left(\frac{x_2}{x_1}\right)+\frac{x_1x_2^2}{x_1^2+x_2^2}. \tag{39}$$

As an illustration, we present the variations of both the material coefficient and the exact potential throughout the sample domain in Figures 9 and 10.

Having used the non-uniform meshes with $m=8, 10, 20$ quadratic elements, we obtained satisfactory and stable results with global percentage errors equal to 0·06721%, 0·06803% and 0·08972%, respectively. It can be seen from Figure 11 that the distribution of the % error falls within an acceptable interval.

5.4. Example 4

To apply the method also to curved geometry, let us consider the BVP governed by Equation (29) in a thick-walled tube with the exponentially graded material coefficient in the radial direction being given by

$$k(\mathbf{x})=k_o e^{\delta(r-a)/(b-a)}, \tag{40}$$

where a and b are the inner and outer radii, respectively.

When the boundary conditions are assumed angularly independent, the problem is rotationally symmetric and the governing equation for such a 1-D problem becomes

$$u''(r)+\left(\frac{1}{r}+\frac{k'}{k}\right)u'(r)=0. \tag{41}$$

Eventually, inserting (40) into (41), we obtain

$$u''(r)+\left(\frac{1}{r}+\gamma\right)u'(r)=0,\quad \gamma=\delta/(b-a). \tag{42}$$

Assuming the potential to be prescribed on both the inner and the outer surfaces, the analytical solution can be expressed as

$$u(r) = u(a) + A \int_a^r \frac{\mathrm{e}^{-\gamma t}}{t} \mathrm{d}t, \tag{43}$$

with $A = [u(b) - u(a)] / \int_a^b \frac{\mathrm{e}^{-\gamma t}}{t} \mathrm{d}t.$

Bearing in mind the definition of the Exponential integral function [31, Chapter 5]

$$E_n(x) = \int_1^\infty \frac{\mathrm{e}^{-xt}}{t^n} \mathrm{d}t, \quad x > 0, \quad n = 0, 1, \ldots \ .$$

we obtain from (43)

$$u(r) = u(a) + \frac{u(b) - u(a)}{E_1(\gamma b) - E_1(\gamma a)} [E_1(\gamma r) - E_1(\gamma a)]. \tag{44}$$

Similarly as in the case of a homogeneous medium, we arrive at

$$u(r) = u(a) + \frac{u(b) - u(a)}{\log b - \log a} [\log r - \log a]. \tag{45}$$

For the numerical evaluation of the Exponential integral function, one can use its continued-fraction representation together with the modified Lentz algorithm [32, Chapter 5.2].

In numerical computations, we have used for values of the material parameter $\delta \in \{0, 0{\cdot}01, 1, 2\}$ and m quadrilateral serendipity elements ($m = 4, 8, 10, 20$) with quadratic approximation. We have discretized a very narrow section given by the angle $\alpha = 10^0$ by using two elements in the angular direction and $m/2$ elements in the radial direction. An illustrative mesh is shown in Figure 12.

The variation of the exponentially graded material coefficient is shown in Figure 5 with the dimensionless coordinate defined now as $x = (r - a)/(b - a)$. Figure 13 shows a good fit to the exact solution by the numerical results similarly as in the case of a square sample. The results have been obtained by using a uniform mesh with eight elements.

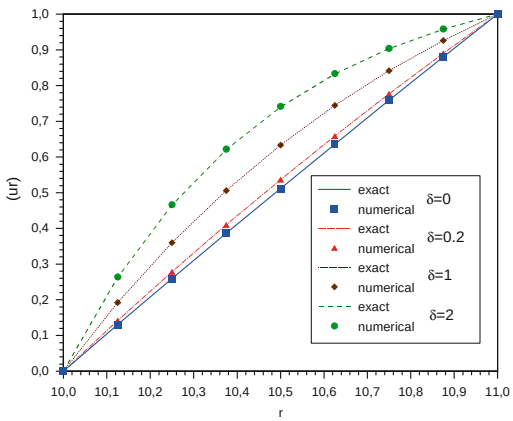

Figure 13. Potential field along the radius of a tube with the exponentially graded material coefficient.

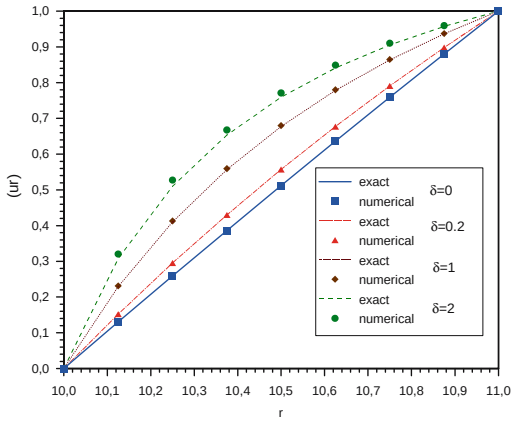

Figure 14. Potential field along the radius of a tube with the power-law graded material coefficient.

5.5. Example 5

Finally, we shall consider a rotationally symmetric problem as in the previous example but with the material coefficient being graded according to the power-law

$$k(r)=\left(1+\delta\frac{r-a}{b-a}\right)^n. \tag{46}$$

Then, the governing equation (41) becomes

$$u''(r)+\left(\frac{1}{r}+\frac{n\gamma}{1+\gamma(r-a)}\right)u'(r)=0 \tag{47}$$

and it can be solved analytically yeilding the result

$$u(r)=u(a)+\frac{u(b)-u(a)}{I(b)-I(a)}[I(r)-I(a)], \tag{48}$$

where $I(r)$ is expressed in terms of elementary functions. For $n=2$, we have

$$I(r)=\frac{1}{A^2}\left[\frac{A}{A+\gamma r}+\log\frac{r}{A+\gamma r}\right], \quad A=1-\gamma a, \quad \gamma=\frac{\delta}{b-a}. \tag{49}$$

The variation of the material coefficient is shown in Figure 7 with the dimensionless coordinate defined as $x=(r-a)/(b-a)$. A comparison of the numerical results with the analytical solution is given in Figure 14. In the case of the worst accuracy ($\delta=2$), the global percentage error is 1·7324 % by using the mesh with eight elements.

Note that all the present results have been obtained by using the collocation of the LIDE only at interior nodes and by satisfying the boundary conditions with approximated fields at the boundary nodes. Alternatively, we have tested also the collocation of the LIDE at the boundary nodes on the Neumann part of the global boundary, but the accuracy of the results has been affected only insignificantly.

6. Conclusions

The paper presents a new formulation for the solution of BVPs in 2-D potential theory in heterogeneous media. This formulation consists in

(i) the domain-type approximation of both the potential field and geometry by using conforming serendipity elements;
(ii) the satisfaction of the prescribed boundary conditions at boundary nodes by approximated fields or alternatively by the collocation of the local integro-differential equations at the boundary nodes on the Neumann part of the global boundary;
(iii) the collocation of the local integro-differential representation of the potential field at interior nodes.

The proposed method is quite general for continuously heterogeneous media, since there is no restriction on the continuous variation of the material coefficient. According to the performed numerical tests, the method is reliable, because of the high accuracy and stability of numerical results. As for as the numerical treatment is concerned, the method is very simple because it uses a simple fundamental solution and non-singular and/or at most weakly-singular integral equations. The system matrix is sparse as in the standard FEM formulation.

In contrast to the weak formulation in the standard FEM, the present formulation is based on the exact integro-differential equations which are solved numerically by using the

same approximation for the primary field as in the FEM. As compared with the boundary-domain formulation, no regularization procedure is required and the approximation concept is inherently consistent. By making use of the domain discretization of the whole structure (together with a reasonable polynomial interpolation of physical fields within domain elements), one can incorporate the complete boundary conditions into the formulation as well as the interaction of the whole bulk of material and the material behaviour in a natural and straightforward way. The discretization mesh prepared in pre-processing can be used successfully also in post-processing of numerical results. Thus, the method can become effective also from the point of view of discretization effort, especially in problems when re-meshing is not required and one needs to know the solution throughout the whole structural domain.

For simplicity, we demonstrated the new formulation using 2-D potential problems. However, the extension of the new formulation to solutions of boundary-value problems for other partial differential equations is possible.

Acknowledgements

The authors acknowledge the support by the Slovak Science and Technology Assistance Agency registered under number APVT-51-003702, as well as by the Slovak Grant Agency VEGA – 2303823, and the Project for Bilateral Cooperation in Science and Technology supported jointly by the International Bureau of the German BMBF and the Ministry of Education of Slovak Republic under the project number SVK 01/020.

Appendix A. Shape functions for some quadrilateral serendipity elements

In this Appendix, we summarize the shape functions and their derivatives for quadrilateral serendipity elements with using the interpolation by Lagrange polynomials. For the bi-linear and bi-quadratic approximations, we present them just for completeness, since they are well known and available from many literature sources. For the sake of brevity, we shall use the notations in which a subscript following a comma denotes the partial derivative, *i.e.*, $N^a_{,i}(\xi_1, \xi_2) = \partial N^a(\xi_1,\xi_2)/\partial\xi_i$, with $(i = 1, 2)$.

(i) *Bi-linear Approximation*

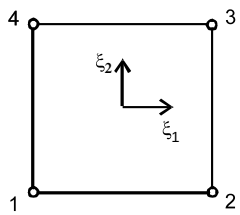

	$a=1$	$a=2$	$a=3$	$a=4$
$N^a(\xi_1,\xi_2)$	$\frac{1}{4}(1-\xi_1)(1-\xi_2)$	$\frac{1}{4}(1+\xi_1)(1-\xi_2)$	$\frac{1}{4}(1+\xi_1)(1+\xi_2)$	$\frac{1}{4}(1-\xi_1)(1+\xi_2)$
$N,^a_1(\xi_1,\xi_2)$	$\frac{1}{4}(\xi_2-1)$	$\frac{1}{4}(1-\xi_2)$	$\frac{1}{4}(1+\xi_2)$	$-\frac{1}{4}(1+\xi_2)$
$N,^a_2(\xi_1,\xi_2)$	$\frac{1}{4}(\xi_1-1)$	$-\frac{1}{4}(1+\xi_1)$	$\frac{1}{4}(1+\xi_1)$	$\frac{1}{4}(1-\xi_1)$

In this case, one can write

$$h^e_{1i}(\xi_1,\xi_2)=a^e_i+\xi_2 b^e_i, \qquad h^e_{2i}(\xi_1,\xi_2)=c^e_i+\xi_1 b^e_i, \tag{A.1}$$

where

$$a^e_i=\left(x^{2e}_i+x^{3e}_i-x^{4e}_i-x^{1e}_i\right)/4, \quad b^e_i=\left(x^{1e}_i-x^{2e}_i+x^{3e}_i-x^{4e}_i\right)/4,$$
$$c^e_i=\left(x^{3e}_i-x^{2e}_i+x^{4e}_i-x^{1e}_i\right)/4.$$

Furthermore,

$$\varepsilon_{3mn}h^e_{1m}h^e_{2n}=f^e+\xi_1 g^e+\xi_2 k^e, \tag{A.2}$$

with

$$f^e=\varepsilon_{3mn}a^e_m c^e_n, \quad g^e=\varepsilon_{3mn}a^e_m b^e_n, \quad k^e=\varepsilon_{3mn}b^e_m c^e_n.$$

Note that $b^e_i=0$ in the case of rectangular bi-linear elements, what enables us to perform all the integrations in LIE analytically.

(ii) *Bi-quadratic Approximation*

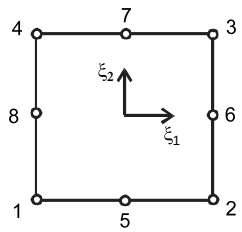

$$N^1=-(1-\xi_1)(1-\xi_2)(\xi_1+\xi_2+1)/4, \quad N^5=(1-\xi_1^2)(1-\xi_2)/2,$$
$$N^2=(1+\xi_1)(1-\xi_2)(\xi_1-\xi_2-1)/4, \quad N^6=(1-\xi_2^2)(1+\xi_1)/2,$$
$$N^3=(1+\xi_1)(1+\xi_2)(\xi_1+\xi_2-1)/4, \quad N^7=(1-\xi_1^2)(1+\xi_2)/2,$$
$$N^4=(1-\xi_1)(1+\xi_2)(-\xi_1+\xi_2-1)/4, \quad N^8=(1-\xi_2^2)(1-\xi_1)/2,$$

$$N^1_{,1}=(1-\xi_2)(2\xi_1+\xi_2)/4, \quad N^5_{,1}=\xi_1(1-\xi_2),$$
$$N^2_{,1}=(1-\xi_2)(2\xi_1-\xi_2)/4, \quad N^6_{,1}=(1-\xi_2^2)/2,$$
$$N^3_{,1}=(1+\xi_2)(2\xi_1+\xi_2)/4, \quad N^7_{,1}=-\xi_1(1+\xi_2),$$
$$N^4_{,1}=(1+\xi_2)(2\xi_1-\xi_2)/4, \quad N^8_{,1}=(\xi_2^2-1)/2.$$

$$N^1_{,2}=(1-\xi_1)(\xi_1+2\xi_2)/4, \quad N^5_{,2}=(\xi_1^2-1)/2,$$
$$N^2_{,2}=(1+\xi_1)(-\xi_1+2\xi_2)/4, \quad N^6_{,2}=-\xi_2(1+\xi_1),$$
$$N^3_{,2}=(1+\xi_1)(\xi_1+2\xi_2)/4, \quad N^7_{,2}=(1-\xi_1^2)/2,$$
$$N^4_{,2}=(1-\xi_1)(-\xi_1+2\xi_2)/4, \quad N^8_{,2}=\xi_2(\xi_1-1).$$

(iii) *Bi-cubic Approximation*

Note that the interpolation polynomials for bi-cubic approximation are rarely published in closed form [33]. We decided to present these polynomials, also because of typing errors in [33, p. 49].

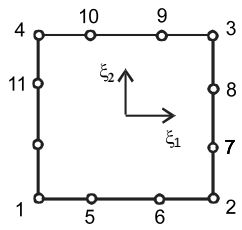

$$N^1=(1-\xi_1)(1-\xi_2)[9(\xi_1^2+\xi_2^2)-10]/32, \qquad N^7=9(1+\xi_1)(1-\xi_2^2)(1-3\xi_2)/32,$$
$$N^2=(1+\xi_1)(1-\xi_2)[9(\xi_1^2+\xi_2^2)-10]/32, \qquad N^8=9(1+\xi_1)(1-\xi_2^2)(1+3\xi_2)/32,$$
$$N^3=(1+\xi_1)(1+\xi_2)[9(\xi_1^2+\xi_2^2)-10]/32 \qquad N^9=9(1+\xi_2)(1-\xi_1^2)(1+3\xi_1)/32,$$
$$N^4=(1-\xi_1)(1+\xi_2)[9(\xi_1^2+\xi_2^2)-10]/32, \qquad N^{10}=9(1+\xi_2)(1-\xi_1^2)(1-3\xi_1)/32,$$
$$N^5=9(1-\xi_2)(1-\xi_1^2)(1-3\xi_1)/32, \qquad N^{11}=9(1-\xi_1)(1-\xi_2^2)(1+3\xi_2)/32,$$
$$N^6=9(1-\xi_2)(1-\xi_1^2)(1+3\xi_1)/32, \qquad N^{12}=9(1-\xi_1)(1-\xi_2^2)(1-3\xi_2)/32.$$

$$N^1_{,1}=(1-\xi_2)[18\xi_1-9(3\xi_1^2+\xi_2^2)+10]/32, \qquad N^7_{,1}=9(1-\xi_2^2)(1-3\xi_2)/32,$$
$$N^2_{,1}=(1-\xi_2)[18\xi_1+9(3\xi_1^2+\xi_2^2)-10]/32, \qquad N^8_{,1}=9(1-\xi_2^2)(1+3\xi_2)/32,$$
$$N^3_{,1}=(1+\xi_2)[18\xi_1+9(3\xi_1^2+\xi_2^2)-10]/32, \qquad N^9_{,1}=9(1+\xi_2)(-9\xi_1^2-2\xi_1+3)/32,$$
$$N^4_{,1}=(1+\xi_2)[18\xi_1-9(3\xi_1^2+\xi_2^2)+10]/32, \qquad N^{10}_{,1}=9(1+\xi_2)(9\xi_1^2-2\xi_1-3)/32,$$
$$N^5_{,1}=9(1-\xi_2)(9\xi_1^2-2\xi_1-3)/32, \qquad N^{11}_{,1}=9(\xi_2^2-1)(1+3\xi_2)/32,$$
$$N^6_{,1}=9(1-\xi_2)(-9\xi_1^2-2\xi_1+3)/32, \qquad N^{12}_{,1}=9(\xi_2^2-1)(1-3\xi_2)/32.$$

$$N^1_{,2}=(1-\xi_1)[18\xi_2-9(\xi_1^2+3\xi_2^2)+10]/32, \qquad N^7_{,2}=9(1+\xi_1)(9\xi_2^2-2\xi_2-3)/32,$$
$$N^2_{,2}=(1+\xi_1)[18\xi_2-9(\xi_1^2+3\xi_2^2)+10]/32, \qquad N^8_{,2}=9(1+\xi_1)(-9\xi_2^2-2\xi_2+3)/32,$$
$$N^3_{,2}=(1+\xi_1)[18\xi_2+9(\xi_1^2+3\xi_2^2)-10]/32, \qquad N^9_{,2}=9(1-\xi_1^2)(1+3\xi_1)/32,$$
$$N^4_{,2}=(1-\xi_1)[18\xi_2+9(\xi_1^2+3\xi_2^2)-10]/32, \qquad N^{10}_{,2}=9(1-\xi_1^2)(1-3\xi_1)/32,$$
$$N^5_{,2}=9(\xi_1^2-1)(1-3\xi_1)/32, \qquad N^{11}_{,2}=9(1-\xi_1)(-9\xi_2^2-2\xi_2+3)/32,$$
$$N^6_{,2}=9(\xi_1^2-1)(1+3\xi_1)/32, \qquad N^{12}_{,2}=9(1-\xi_1)(9\xi_2^2-2\xi_2-3)/32.$$

(iv) *Bi-quartic Approximation*

We have never seen published in closed form the interpolation polynomials for biquartic approximation. That is why, we present them here.

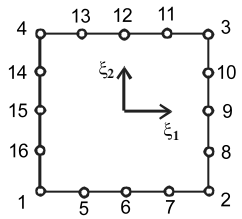

$$N^1=(1-\xi_1)(1-\xi_2)/4-3(N^5+N^{16})/4-(N^6+N^{15})/2-(N^7+N^{14})/4,$$
$$N^2=(1+\xi_1)(1-\xi_2)/4-3(N^7+N^8)/4-(N^6+N^9)/2-(N^5+N^{10})/4,$$
$$N^3=(1+\xi_1)(1+\xi_2)/4-3(N^{10}+N^{11})/4-(N^9+N^{12})/2-(N^8+N^{13})/4,$$
$$N^4=(1-\xi_1)(1+\xi_2)/4-3(N^{13}+N^{14})/4-(N^{12}+N^{15})/2-(N^{11}+N^{16})/4,$$
$$N^5=4\xi_1(1-\xi_1^2)(\xi_1-1/2)(1-\xi_2)/3, \qquad N^{11}=4\xi_1(1-\xi_1^2)(\xi_1+1/2)(1+\xi_2)/3,$$
$$N^6=2(\xi_1^2-1)(\xi_1^2-1/4)(1-\xi_2), \qquad N^{12}=2(\xi_1^2-1)(\xi_1^2-1/4)(1+\xi_2),$$
$$N^7=4\xi_1(1-\xi_1^2)(\xi_1+1/2)(1-\xi_2)/3, \qquad N^{13}=4\xi_1(1-\xi_1^2)(\xi_1-1/2)(1+\xi_2)/3,$$
$$N^8=4\xi_2(1-\xi_2^2)(\xi_2-1/2)(1+\xi_1)/3, \qquad N^{14}=4\xi_2(1-\xi_2^2)(\xi_2+1/2)(1-\xi_1)/3,$$
$$N^9=2(\xi_2^2-1)(\xi_2^2-1/4)(1+\xi_1), \qquad N^{15}=2(\xi_2^2-1)(\xi_2^2-1/4)(1-\xi_1),$$
$$N^{10}=4\xi_2(1-\xi_2^2)(\xi_2+1/2)(1+\xi_1)/3, \qquad N^{16}=4\xi_2(1-\xi_2^2)(\xi_2-1/2)(1-\xi_1)/3.$$

$$N^1_{,1}=(\xi_2-1)/4-3(N^5_{,1}+N^{16}_{,1})/4-(N^6_{,1}+N^{15}_{,1})/2-(N^7_{,1}+N^{14}_{,1})/4,$$
$$N^2_{,1}=(1-\xi_2)/4-3(N^7_{,1}+N^8_{,1})/4-(N^6_{,1}+N^9_{,1})/2-(N^5_{,1}+N^{10}_{,1})/4,$$
$$N^3_{,1}=(1+\xi_2)/4-3(N^{10}_{,1}+N^{11}_{,1})/4-(N^9_{,1}+N^{12}_{,1})/2-(N^8_{,1}+N^{13}_{,1})/4,$$
$$N^4_{,1}=-(1+\xi_2)/4-3(N^{13}_{,1}+N^{14}_{,1})/4-(N^{12}_{,1}+N^{15}_{,1})/2-(N^{11}_{,1}+N^{16}_{,1})/4,$$

$$N^5_{,1}=4(1-\xi_2)[(1-3\xi_1^2)(\xi_1-1/2)+\xi_1(1-\xi_1^2)]/3, \qquad N^6_{,1}=(1-\xi_2)\xi_1(8\xi_1^2-5),$$
$$N^7_{,1}=4(1-\xi_2)[(1-3\xi_1^2)(\xi_1+1/2)+\xi_1(1-\xi_1^2)]/3, \qquad N^8_{,1}=4\xi_2(1-\xi_2^2)(\xi_2-1/2)/3,$$
$$N^9_{,1}=2(\xi_2^2-1)(\xi_2^2-1/4), \qquad N^{10}_{,1}=4\xi_2(1-\xi_2^2)(\xi_2+1/2)/3,$$
$$N^{11}_{,1}=4(1+\xi_2)[(1-3\xi_1^2)(\xi_1+1/2)+\xi_1(1-\xi_1^2)]/3, \qquad N^{12}_{,1}=(1+\xi_2)\xi_1(8\xi_1^2-5),$$
$$N^{13}_{,1}=4(1+\xi_2)[(1-3\xi_1^2)(\xi_1-1/2)+\xi_1(1-\xi_1^2)]/3, \qquad N^{14}_{,1}=4\xi_2(\xi_2^2-1)(\xi_2+1/2)/3,$$
$$N^{15}_{,1}=2(1-\xi_2^2)(\xi_2^2-1/4), \qquad N^{16}_{,1}=4\xi_2(1-\xi_2^2)(1/2-\xi_2)/3.$$

$$N^1_{,2}=(\xi_1-1)/4-3(N^5_{,2}+N^{16}_{,2})/4-(N^6_{,2}+N^{15}_{,2})/2-(N^7_{,2}+N^{14}_{,2})/4,$$
$$N^2_{,2}=-(1+\xi_1)/4-3(N^7_{,2}+N^8_{,2})/4-(N^6_{,2}+N^9_{,2})/2-(N^5_{,2}+N^{10}_{,2})/4,$$
$$N^3_{,2}=(1+\xi_1)/4-3(N^{10}_{,2}+N^{11}_{,2})/4-(N^9_{,2}+N^{12}_{,2})/2-(N^8_{,2}+N^{13}_{,2})/4,$$
$$N^4_{,2}=(1-\xi_1)/4-3(N^{13}_{,2}+N^{14}_{,2})/4-(N^{12}_{,2}+N^{15}_{,2})/2-(N^{11}_{,2}+N^{16}_{,2})/4,$$

$$N^5_{,2}=4\xi_1(1-\xi_1^2)(1/2-\xi_1)/3, \qquad N^6_{,2}=2(1-\xi_1^2)(\xi_1^2-1/4),$$
$$N^7_{,2}=4\xi_1(\xi_1^2-1)(\xi_1+1/2)/3, \qquad N^8_{,2}=4(1+\xi_1)[(1-3\xi_2^2)(\xi_2-1/2)+\xi_2(1-\xi_2^2)]/3,$$
$$N^9_{,2}=(1+\xi_1)\xi_2(8\xi_2^2-5), \qquad N^{10}_{,2}=4(1+\xi_1)[(1-3\xi_2^2)(\xi_2+1/2)+\xi_2(1-\xi_2^2)]/3,$$
$$N^{11}_{,2}=4\xi_1(1-\xi_1^2)(\xi_1+1/2)/3, \qquad N^{12}_{,2}=2(\xi_1^2-1)(\xi_1^2-1/4),$$
$$N^{13}_{,2}=4\xi_1(1-\xi_1^2)(\xi_1-1/2)/3, \qquad N^{14}_{,2}=4(1-\xi_1)[(1-3\xi_2^2)(\xi_2+1/2)+\xi_2(1-\xi_2^2)]/3,$$
$$N^{15}_{,2}=(1-\xi_1)\xi_2(8\xi_2^2-5), \qquad N^{16}_{,2}=4(1-\xi_1)[(1-3\xi_2^2)(\xi_2-1/2)+\xi_2(1-\xi_2^2)]/3.$$

References

1. T. Hirai, Functionally gradient materials, In: R.J. Brook(ed.), *Material Science and Technology, Vol. 17B, Processing of Ceramics, Part 2*. Weinheim, Germany (1993) pp. 292–341.
2. G.H. Paulino, Z.H. Jin and R.H. Dodds Jr., Failure of functionally graded materials. In: B.L. Karihaloo and W.G. Knauss (eds.), *Comprehensive Structural Integrity, Vol. 2, Chap. 13*. Oxford: Elsevier Science Ltd. (2003) in print.
3. S. Suresh and A. Mortensen, *Fundamentals of Functionally Graded Materials*. London: The Institute of Materials (1998) 165 pp.
4. Y. Miyamoto, W.A. Kaysser, B.H. Rabin, A. Kawasaki and R.G. Ford, *Functionally Graded Materials, Design, Processing and Applications*. Dordrecht : Kluwer Academic Publishers (1999) 330 pp.
5. J.H. Kim and G.H. Paulino, Isoparametric graded finite elements for nonhomogeneous isotropic and orthotropic materials. *J. Appl. Mech. Trans. ASME* 69 (2002) 502–514.
6. M. Tanaka and K. Tanaka, Transient heat conduction problems in inhomogeneous media discretized by means of boundary-volume element. *Nucl. Eng. Des.* 60 (1980) 381–387.
7. V. Sladek, J. Sladek and I. Markechova, An advanced boundary element method for elasticity in nonhomogeneous media. *Acta Mech.* 97 (1993) 71–90.
8. V. Sladek and J. Sladek, A new formulation for solution of boundary value problems using domain-type approximations and local integral equations. *Electr. J. Bound. Elem.* 1 (2003) 132–153.
9. D.L. Clements, A boundary integral equation method for the numerical solution of a second order elliptic equation with variable coefficients. *J. Aust. Math. Soc. Ser. B* 22 (1980) 218–228.
10. A.H.-D. Cheng, Darcy's flow with variable permeability – a boundary integral solution. *Water Resour. Res.* 20 (1984) 980–984.
11. A.H.-D. Cheng, Heterogeneities in flows through porous media by boundary element method. In: *Topics in Boundary Element Research Vol. 4. Applications to Geomechanics*. (1987) pp. 1291–1344.
12. R.P. Shaw and N. Makris, Green's functions for Helmholtz and Laplace equations in heterogeneous media. *Eng. Anal. Bound. Elem.* 10 (1992) 179–183.
13. R.P. Shaw, Green's functions for heterogeneous media potential problems. *Eng. Anal. Bound. Elem.* 13 (1994) 219–221.
14. W.T. Ang, J. Kusuma and D.L. Clements, A boundary element method for a second order elliptic partial differential equation with variable coefficients. *Eng. Anal. Bound. Elem.* 18 (1986) 311–316.
15. L.J. Gray, T. Kaplan, J.D. Richardson and G.H. Paulino, Green's functions and boundary integral analysis for exponentially grded materials: Heat conduction. *J. Appl. Mech. Trans. ASME* 70 (2003) 543–549.
16. P.A. Martin, J.D. Richardson, L.J. Gray and J.R. Berger, On Green's function for a three-dimensional exponentially-graded elastic solid. *Proc. Roy. Soc. London* A 458 (2002) 1931–1947.
17. Y.-S. Chan, L.J. Gray, T. Kaplan and G.H. Paulino, Green's function for a two-dimensional exponentially-graded elastic medium. *Proc. Roy. Soc. London* A 460 (2003) 1689–1706.
18. J. Sladek, V. Sladek and S.N. Atluri, Local boundary integral equation (LBIE) method for solving problems of elasticity with nonhomogeneous material properties. *Comp. Mech.* 24 (2000) 456–462.
19. J. Sladek, and V. Sladek, Local boundary integral equation method for heta conduction problem in an anisotropic medium. In: C.A. Herrera, (ed.), *Advances in Computational and Experimental Engineering & Sciences CD – Proc. Conf. ICCES* 2003, Corfu, Greece (2003).
20. J. Sladek, V. Sladek and Ch. Zhang, A local BIEM for analysis of transient heat conduction with nonlinear source terms in FGMs. *Eng. Anal. Bound. Elem.* 28 (2003) pp. 1–11.

21. J. Sladek, V. Sladek and Ch. Zhang, Transient heat conduction analysis in functionally graded materials by meshless local boundary integral equation method. *Comput. Mater. Sci.* 28 (2003) 494–504.
22. J. Sladek, V. Sladek, J. Krivacek and Ch. Zhang, Local BIEM for transient heat conduction analysis in 3-D axisymmetric functionally graded solids. *Comp. Mech.* 32 (2003) 169–176.
23. J. Sladek, V. Sladek and Ch. Zhang, Application of meshless Petrov-Galerkin (MLPG) method to elastodynamic problems in continuously nonhomogeneous solids. *Comp. Model. Eng. Sci.* 4 (2003) 637–647.
24. V. Sladek and J. Sladek, Global and local integral equations for potential problems in non-homogeneous media. *CTU Report* 4 (2000) 133–138.
25. V. Sladek, J. Sladek and R. Van Keer: New integral equation approach to solution of diffusion equation. In: V. Kompis, M. Zmindak and E.A.W. Maunder, (eds.), *CD-Proc. of the 8*th *Int. Conf. on Numerical Methods in Continuum Mechanics*, Univ. of Zilina, Slovakia (2000).
26. V. Sladek, J. Sladek and R. Van Keer, New integral equation approach to solution of diffusion equation. *Comp. Assist. Mech. Engn. Sci*. 9 (2002) 555–572.
27. V. Sladek, J. Sladek and Ch. Zhang, Local integral equations treatment of potential problems in non-homogeneous media. In: V. Kompis and M. Zmindak, (eds.), *Numerical Methods in Continuum Mechanics. CD-Proc. of the 9th Int. Conf. NMCM 2003*, Zilina, Slovakia, ISBN 80-968823-4-1 (2003).
28. S.E. Mikhailov, Localized boundary-domain integral formulations for problems with variable coefficients. *Eng. Anal. Bound. Elem.* 26 (2002) 681–690.
29. S.E. Mikhailov and I.S. Nakhova, Numerical solution of a Neumann problem with variable coefficients by the localized boundary-domain integral equation method. In: Sia Amini (ed.), *Fourth UK Conf. on Boundary Integral Methods*. Salford University, UK, ISBN 0-902896-40-7, (2003) 175–184.
30. L.C. Wrobel, *The Boundary Element Method, Vol. 1: Applications in Thermo-Fluids and Acoustics*. Chichester: John Wiley & Sons (2002) 451 pp.
31. M. Abramowitz and I.A. Stegun, *Handbook of Mathematical Functions, Applied Mathematics Series*. New York: Dover Publications (1964) 1046 pp.
32. W.H. Press, S.A. Teukolsky, W.T. Vetterling, and B.P. Flannery, *Numerical Recipes in C: The Art of Scientific Computing*. Cambridge University Press (1988–1992) 1032 pp.
33. M.H. Aliabadi, *The Boundary Element Method, Vol. 2: Applications in Solids and Structures*. Chichester: John Wiley & Sons (2002) 580 pp.